# RESEARCH ARTICLE

# Enhanced Luminescent Performance via Passivation of Surface Undercoordinated Pb Atoms in a CsPbBr₃ Microplate

*Yizhi Zhu, Linlin Shi, Heng Guo, Jinping Chen, Junfeng Lu, Weian Wang, Zhangsheng Xu, Naiwei Gao, Xun Han, Zhengchun Peng,\* Qiannan Cui, Chunxiang Xu,\* and Caofeng Pan\**

Perovskite materials are widely used in the fields of luminescence and light energy conversion with the advantages of low cost and outstanding optoelectronic properties. However, abundant surface lattice defects heavily affect the performances of perovskite optoelectronic devices. Here, by treating surface defects with oleylamine molecules in situ, the surface trap states are significantly decreased in a CsPbBr₃ microplate, enabling photoluminescence intensity and carrier lifetimes to be dramatically enhanced and prolonged, respectively. These interesting phenomena can be attributed to the binding of undercoordinated Pb atoms with N atoms on the surface of perovskite microplate. The strong binding energy of lead-halogen bonds inhibits the photodegraded reactions of the crystal, leading to the significant improvement of luminescent stability for the microplate correspondingly. The results not only provide experimental guidance for passivating lattice defects but also pave the way for improving the efficiency of wide materials and optoelectronic devices.

## 1. Introduction

Due to low fabrication cost and excellent optoelectronic performances, solution-processable lead halide perovskites have been extensively applied in the fields of solar cells,[1–6] photodetectors,[7–10] transistors,[11–13] and so on. So far, the energy conversion efficiency of perovskite solar cells has exceeded 25%,[14–16] superior to polycrystalline silicon solar cells, but this value is still far below the theoretical efficiency limit. In addition, benefiting from outstanding luminescent properties and tunable emission wavelengths,[17] perovskite has also attracted great attention in luminescence applications, such as light-emitting diodes (LEDs)[18–20] and optically pumped lasers.[21–24] Although perovskite materials have achieved above remarkable progress in the application of optoelectronic devices,[25–30] the efficiency of these devices still needs to be further improved and optimized urgently, to match the practical application.[31–37]

Solution-processed perovskite tends to form abundant lattice defects because of low crystal nucleus formation energy.[38,39] The existence of abundant surface lattice defects plays a vital role in the performances of perovskite optoelectronic devices.[31,32,40–42] First of all, lattice defects can cause carriers trap states in momentum space,[43] and the formed trap states will heavily dissipate the energies of photocarriers

Y. Zhu, N. Gao, Z. Peng, C. Pan
College of Physics and Optoelectronic Engineering
Shenzhen University
Shenzhen 518060, P. R. China
E-mail: zcpeng@szu.edu.cn; cfpan@binn.cas.cn

Y. Zhu, Z. Xu, C. Pan
CAS Center for Excellence in Nanoscience
Beijing Key Laboratory of Micro-nano Energy and Sensor
Beijing Institute of Nanoenergy and Nanosystems
Chinese Academy of Sciences
Beijing 101400, P. R. China

L. Shi
College of Physics and Optoelectronics
Key Lab of Advanced Transducers and Intelligent Control System of Ministry of Education
Taiyuan University of Technology
Taiyuan 030024, P. R. China

H. Guo, J. Chen, W. Wang, Q. Cui, C. Xu
State Key Laboratory of Bioelectronics
School of Biological Science and Medical Engineering
Southeast University
Nanjing 210096, P. R. China
E-mail: xcxseu@seu.edu.cn

J. Lu
College of Science
Nanjing University of Aeronautics and Astronautics
Nanjing 211106, P. R. China

X. Han
College of Mechatronics and Control Engineering
Shenzhen University
Shenzhen 518060, P. R. China

into heat through a non-radiative recombination process.[40,44] It is a serious problem that hinders the performance of perovskites-based optoelectronic devices.[32,39] The other serious problem is that the crystal structures of perovskites can be decomposed by water, oxygen, and heating.[45,46] Previous works have shown that surface lattice defects in perovskite can deeply affect crystal stability and hinder the device's service lifespan by accelerating the photodegraded reactions mediated with $H_2O$ and $O_2$.[47,48] Therefore, surface lattice defects are one of the essential factors that restrict the performance of perovskite optoelectronic devices.

In this paper, aiming to improve luminescent performances and reduce non-radiative energy loss, OLA molecules are employed to passivate surface lattice defects of the $CsPbBr_3$ microplates. Results have shown that OLA molecules can effectively decrease surface trap states via passivating undercoordinated $Pb^{2+}$ ions. Thus, both the PL intensity and the carrier's lifetime of OLA-$CsPbBr_3$ are enhanced and prolonged compared with pure $CsPbBr_3$ microplate. In addition, the luminescent stability of the microplates is also significantly improved after passivating the undercoordinated Pb atoms by OLA molecules. Our results are significant for an extensive range of high-efficiency perovskite materials and devices.

## 2. Results and Discussion

### 2.1. Experimental Design and Structural Analysis

First, an optical system has been built by connecting a PL spectrometer and a streak camera (see **Figure 1**a) to investigate the luminescent performance of a perovskite microcrystal. A 400 nm laser beam is adopted as the excitation source, which is focused on a $CsPbBr_3$ microplate by an objective lens with an NA of 0.4. The emitted PL from the microplate is split into two beams by a beam splitter. One beam is recorded with a spectrometer for PL analysis, and the other one is sent to a streak camera for carrier dynamics measurement. By successfully constructing this optical measurement system, we can precisely investigate the PL and TRPL of a perovskite microplate. The experimental design for surface passivation of a $CsPbBr_3$ microplate is depicted in Figure 1b. As presented in Figure 1b, we attempt to passivate surface lattice defects with OLA molecules and a microplate ultimately achieves excellent luminescent performance. Moreover, the structure and morphology of solution-fabricated microplates are measured with X-ray diffractometry (XRD) and scanning electron microscopy (SEM) equipped with an energy dispersive spectroscopy (EDS), respectively, as shown in Figure 1c–e. The synthesized $CsPbBr_3$ microplates demonstrate a smooth surface and sharp edges with a square shape, indicating excellent crystalline quality. In addition, Cs, Pb, and Br elements are uniformly distributed on the crystal surface. It indicates that we have successfully fabricated high-quality $CsPbBr_3$ microplates by the solution-synthesized method.

### 2.2. Trap Density and Exciton Dynamics

Next, a series of steady micro-PL spectra on a 200 nm thick $CsPbBr_3$ microplate is measured to quantitively estimate trap density (The details of the thickness of $CsPbBr_3$ microplates can be seen in the Supporting Information). **Figure 2**a shows
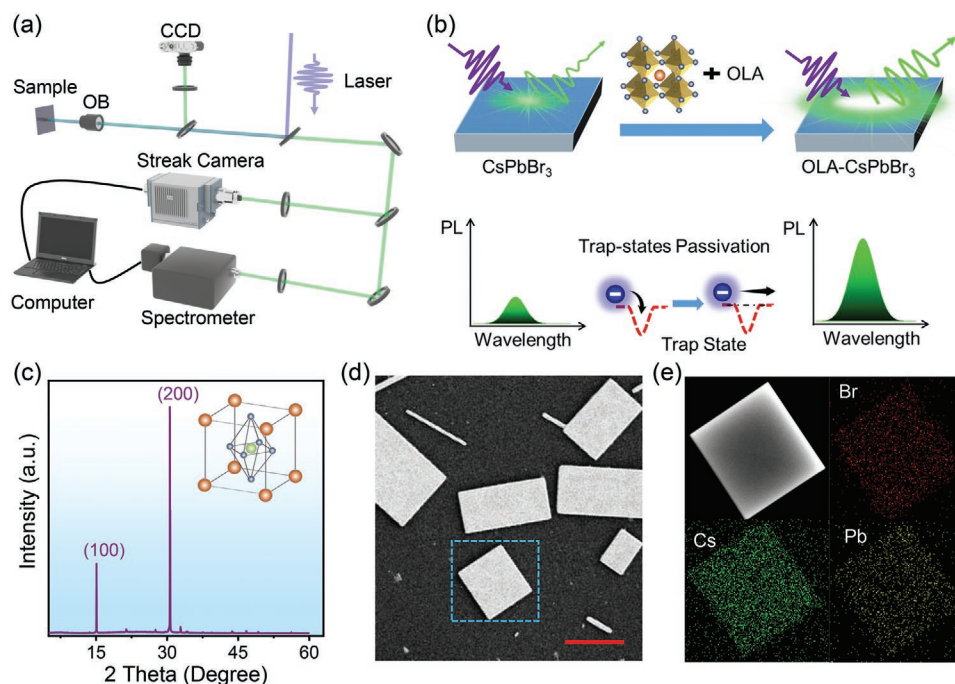


**Figure 1.** Testing setup, experimental design, and structural measurement of the $CsPbBr_3$ microplates. a) The optical path for measuring PL and time-resolved photoluminescence (TRPL) spectra emitted from a $CsPbBr_3$ microplate. b) A schematic diagram for surface passivation design. c) The XRD pattern of the as-synthesized $CsPbBr_3$ microplates. The inset shows the crystal structure of $CsPbBr_3$. d) An SEM image of solution-synthesized $CsPbBr_3$ microplates with a scale bar of 10 μm. e) The elemental mapping of Cs, Pb, and Br for a microplate.
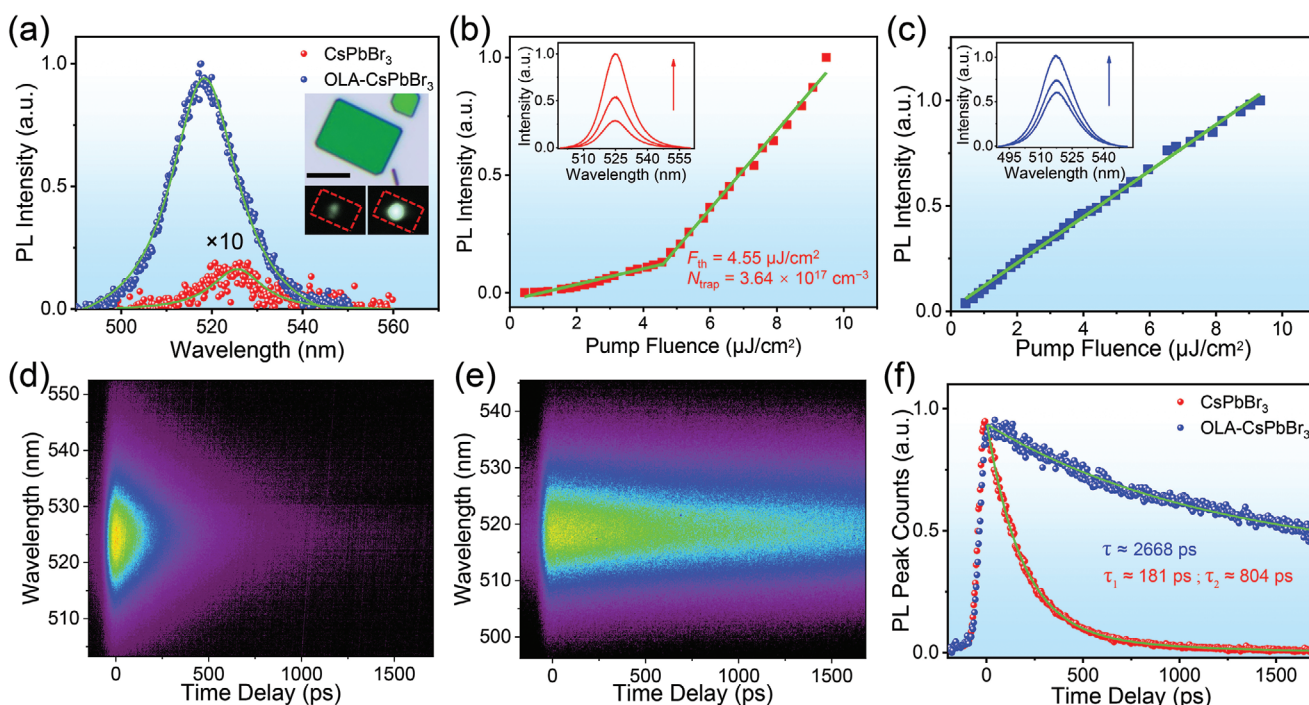
**Figure 2.** The measurement of micro-PL and micro-TRPL spectra for a CsPbBr$_3$ microplate in situ. a) Steady PL spectra for a CsPbBr$_3$ microplate with and without OLA molecules. Corresponding insets show bright and dark fields of optical images of the CsPbBr$_3$ microplate with 10 μm scale bars. Excitation fluence of a 400 nm femtosecond laser beam is fixed at 0.44 μJ cm$^{-2}$. PL intensity as a function of pump fluence is presented for b) CsPbBr$_3$ and c) OLA-CsPbBr$_3$ microplate. Solid lines are linear fittings. Insets are the three typical PL spectra for the two samples. Typical TRPL spectra for d) CsPbBr$_3$ and e) OLA-CsPbBr$_3$ microplate, and f) temporal decay of PL intensity at PL peak extracted from (d) and (e) when excitation fluence is fixed at 3.82 μJ cm$^{-2}$. The green lines in (f) for CsPbBr$_3$ and OLA-CsPbBr$_3$ are bi-exponential and exponential fittings, respectively.

the PL spectra of the CsPbBr$_3$ microplate with and without OLA molecules. It shows that the PL intensity of OLA-CsPbBr$_3$ is remarkably enhanced by about 70-folds than the pure CsPbBr$_3$ microplate. Inset in Figure 2a is the bright field optical image of the microplate, it shows a greenish CsPbBr$_3$ microplate with a length of about 10 μm. And it is clear that under the excitation of the 400 nm laser, much higher luminescence radiation is observed by a charge-coupled device (CCD) when OLA molecules are employed on the CsPbBr$_3$ microplate, which agrees well with PL enhancement results as shown in Figure 2a. It suggests that OLA molecules can effectively improve the luminescence performances of CsPbBr$_3$. Moreover, we can find that the fitted PL peak of OLA-CsPbBr$_3$ is located at 518.28 nm, exhibiting an obvious blueshift of 6.96 nm compared with pure CsPbBr$_3$ (525.24 nm) recorded by a Princeton Instrument Spectrometer (Supporting Information). Therefore, we can infer that there is a stronger interaction between CsPbBr$_3$ and OLA molecules.

To reveal this conjecture, we carefully performed pump power-dependent steady micro-PL of the CsPbBr$_3$ microplate with and without OLA molecules treatment. Figure 2b presents the PL intensity of CsPbBr$_3$ as a function of pump fluences, and pump fluences of red-solid spectra in the inset are 3.60, 4.55, and 5.80 μJ cm$^{-2}$. It indicates that the PL intensity exhibit two linear growth trends with a threshold of 4.55 μJ cm$^{-2}$. Based on a trap-filling model,[39,40,49] the photogenerated band-edge excitons can be captured by trap states when the pump fluence is low. After trap states are filled, a large number of excess

excitons at the band-edge will emit PL by the path of radiative recombination. Thus, the quantum efficiency and PL intensity are suddenly increased. Figure 2b shows the threshold obtained by fitting the scatter plot through two linear functions which can be approximately adopted to calculate the average trap density. Therefore, when the pump fluence threshold is 4.55 μJ cm$^{-2}$, the trap density of the CsPbBr$_3$ microplate can be estimated to be $3.64 \times 10^{17}$ cm$^{-3}$ (Supporting Information). The PL intensity of CsPbBr$_3$ as a function of pump fluences is shown in Figure 2c and pump fluences of blue-solid spectra in the inset are 3.60, 4.66, and 5.95 μJ cm$^{-2}$. It is noticed that the trap density of OLA-CsPbBr$_3$ is significantly decreased, approaching the ideal defect-free conditions, as indicated by Figure 2c. These results prove that the OLA molecules can effectively passivate surface lattice defects on the CsPbBr$_3$ microplate.

Then, the micro-TRPLs of the microplate before and after surface passivating treatment with OLA are measured by a streak camera to further elaborate exciton dynamics. TRPL spectra of OLA-CsPbBr$_3$ present a significantly longer tail along the temporal axial than the pure CsPbBr$_3$, as shown in Figure 2d,e. It shows that OLA-CsPbBr$_3$ possesses a longer PL lifetime compared with pure CsPbBr$_3$. To better understand exciton dynamics in CsPbBr$_3$, temporal dynamics of PL peaks are extracted from Figure 2d,e, as plotted in Figure 2f. For a pure CsPbBr$_3$ microplate, indicated by the red sphere, we fit this PL peak with a bi-exponential function: $I = A_1 e^{-\frac{t}{\tau_1}} + A_2 e^{-\frac{t}{\tau_2}}$, where $A_1$ ($A_2$) is constants, $\tau_1$ and $\tau_2$ are fast and slow PL decay

components, respectively. The fitted $A_1$ and $A_2$ are 0.87 and 0.09, and $\tau_1$ and $\tau_2$ are about 181 and 804 ps, respectively. Furthermore, the average PL lifetime of the CsPbBr$_3$ is 377 ps calculated by $\tau_{avg} = (A_1\tau_1^2 + A_2\tau_2^2)/(A_1\tau_1 + A_2\tau_2)$. Previous works have reported that fast ($\tau_1$) and slow ($\tau_2$) PL decay components are intrinsically originated from the exciton recombination process in the surface and bulk regions of a CsPbBr$_3$ microplate with inhomogeneous trap densities.[39,50] Thus, we can safely estimate the proportion of PL emission in the surface region is about 68.5%, which is calculated by $A_1\tau_1/(A_1\tau_1 + A_2\tau_2)$. Since OLA-CsPbBr$_3$ exhibits defect-free properties as shown in Figure 2c, we empirically interpreted the PL peak of OLA-CsPbBr$_3$ with an exponential function: $I = Ae^{-\frac{t}{\tau}}$. It exhibited that the fitted $\tau$ of OLA-CsPbBr$_3$ equals 2668 ps as seen in Figure 2f. It concludes that the PL lifetime of OLA-CsPbBr$_3$ is ≈7 times longer than the pure CsPbBr$_3$, indicating an excellent surface passivation effect, which agrees well with the results in Figure 2b,c. In addition, it is observed that the temporal-integrated PL spectrum (0–1700 ps, temporally recorded by an Optronics Streak Camera and see the Supporting Information) of OLA-CsPbBr$_3$ is blueshifted by 5.66 nm compared with the pure CsPbBr$_3$. This result is satisfactorily consistent with Figure S1 (Supporting Information) by a measurement error of 1 nm, confirming the high quality of our steady PL and TRPL measurements.

From PL and TRPL results, two spectroscopic features can be summarized: 1) PL intensity is remarkably enhanced while defects are efficiently passivated by OLA molecules. 2) Benefitting from the decrease of trap states, the PL lifetime of OLA-CsPbBr$_3$ is prolonged significantly. Based on these features, we proposed a schematic illustration to interpret carrier dynamics in the CsPbBr$_3$-based microplate. As depicted in **Figure 3**a, abundant surface lattice defects in a pure CsPbBr$_3$ microplate can generate carrier trap states in momentum space, leading

to the capture of free carriers by defects and the dissipation of energy into heat during their paths of energy relaxations. Thus, the microplate presents poor PL performance and a rather short PL lifetime caused by heavy surface recombinations. When OLA is introduced on the surface of the microplate, trap states are significantly reduced because of the passivation of surface defects with OLA molecules, as shown in Figure 3b. Since the passivation of OLA molecules decreases the surface recombination of carriers, PL performance and carrier lifetime of OLA-CsPbBr$_3$ are enhanced and prolonged respectively. It indicates that OLA molecules can effectively decrease surface recombination by passivating surface trap states of the perovskite.

## 2.3. Surface Elemental Analysis

According to the exciton dynamics results, it can be inferred that OLA molecules can passivate the lattice defects on the surface of pure CsPbBr$_3$ microplate. Since the N atom exists at the amine head of OLA molecule, we can expect that the passivation mechanism of the OLA molecule is similar to that of Lewis bases where lone pair of electrons hang outside to N atoms. So the lone pair can bind with an undercoordinated Pb atom at the surface of perovskite to passivate the lattice defects, as shown in **Figure 4**a. To further elucidate the passivation mechanism, the XPS spectra of OLA, pure CsPbBr$_3$, and OLA-CsPbBr$_3$ are measured, respectively, as shown in Figure 4b. The peaks of Cs, Pb, and Br elements are observed from both pure CsPbBr$_3$ and OLA-CsPbBr$_3$ microplates, while the N element is detected at the surface of OLA-CsPbBr$_3$, suggesting that the OLA molecules are successfully bonded to the surface of pure CsPbBr$_3$ microplates. XPS high-resolution spectra of Cs 3d, Br 3d, and Pb 4f on pure CsPbBr$_3$ and OLA-CsPbBr$_3$ are extracted and presented in Figure 4c–e, respectively. It can be seen that
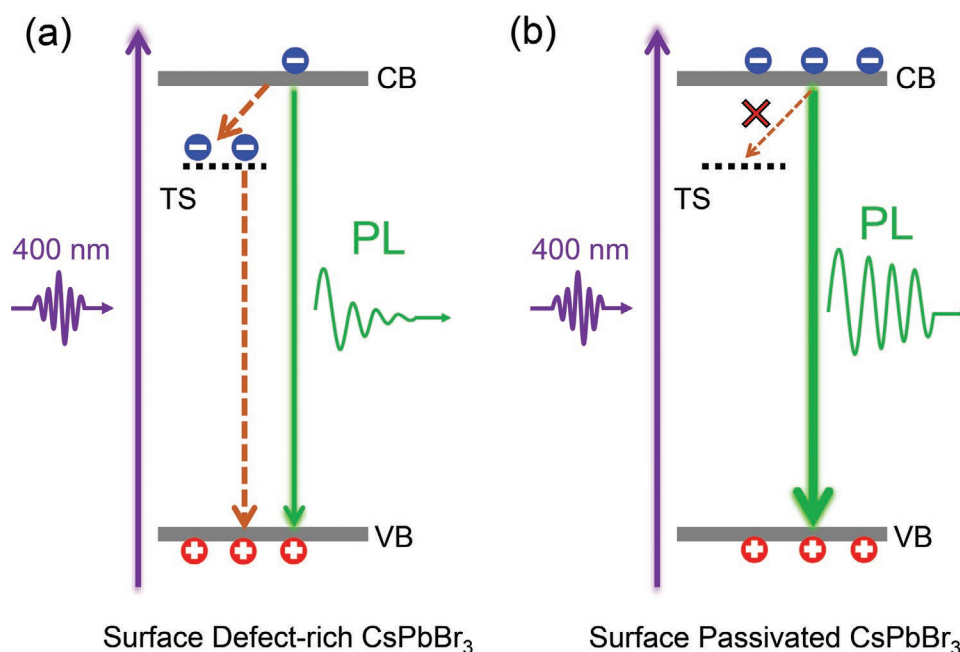


**Figure 3.** Schematic illustration of trap-state-mediated carrier dynamics. Photogenerated carrier relaxation process in a) a pure CsPbBr$_3$ and b) surface passivated CsPbBr$_3$ microplate.

**ADVANCED
SCIENCE NEWS**

www.advancedsciencenews.com
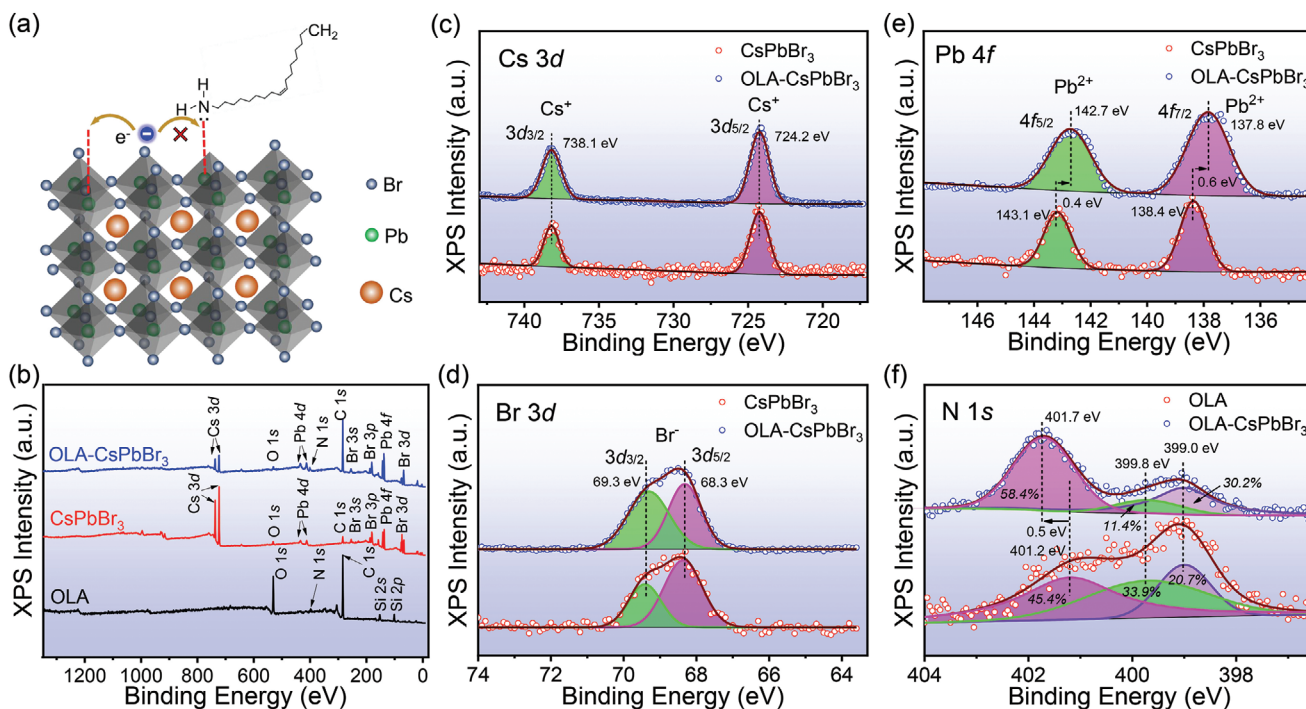
**ADVANCED
OPTICAL
MATERIALS**

www.advopticalmat.de

**Figure 4.** XPS survey and high-resolution spectra. a) The possible passivation mechanism between OLA molecules and pure $CsPbBr_3$ microplate. b) XPS survey spectra of OLA, pure $CsPbBr_3$, and OLA-$CsPbBr_3$. High-resolution XPS c) Cs 3d, d) Br 3d, and e) Pb 4f of pure $CsPbBr_3$ and OLA-$CsPbBr_3$. f) High-resolution XPS N 1s of OLA and OLA-$CsPbBr_3$.

the binding energy of Cs 3d and Br 3d in OLA-$CsPbBr_3$ have no shift compared with pure $CsPbBr_3$. However, XPS peaks of Pb 4f7/2 and 4f5/2 are shifted toward the lower binding energy region by 0.6 and 0.4 eV after OLA passivating, respectively. It suggests that the undercoordinated Pb atom can bond with OLA, and receive electrons from OLA molecules.

To further reveal the passivation mechanism, we measured the XPS high-resolution spectra of N in OLA and OLA-$CsPbBr_3$, respectively. As shown in Figure 4f, the binding energies of N for pure chemical OLA are located at 401.2, 399.8, and 399.0 eV, corresponding to the lone pair of N atom,[51,52] $-NH_2$[53,54] and N$-$O[55,56] bond, respectively. The N$-$O bond is likely to be caused by oxidation of the amine head during the measurement. However, the binding energies of N in OLA-$CsPbBr_3$ are located at 401.7, 399.8, and 399.0 eV, respectively. Compared with pure OLA molecules, the peak of $NH_3^+$ is shifted to a high binding energy region by 0.5 eV on the surface of OLA-$CsPbBr_3$ microplates, and its ratio increases from 45.4% to 58.4%. It further reveals that the N atom in OLA interacts with surface defects on perovskite by donating electrons. Combined with the results in Figure 4e,f, we can safely conclude that the passivation mechanism of OLA-$CsPbBr_3$ is that the undercoordinated Pb atom on pure $CsPbBr_3$ can be bonded with the N atom of OLA molecule. These experimental results are consistent with the expected possible passivation mechanism as shown in Figure 4a. It has been reported that surface lattice defects of pure $CsPbBr_3$ mainly include undercoordinated bonds, such as $Pb^{2+}$ and $Br^-$ ions.[57] Lewis acids and Lewis bases can specifically passivate the undercoordinated $Pb^{2+}$, $Br^-$, and other chemical bonds, respectively.[57,58] Since the structure of OLA

molecules is like Lewis bases, the lone pair on the terminal N atom can bind to the $Pb^{2+}$ bond with a lead-halogen bond,[59,60] ultimately passivate the surface defects of perovskite crystals. It is to be mentioned that our results are consistent with the previously reported passivation mechanism of Lewis bases.

Based on the XPS high-resolution spectra, the XPS valence band spectra of pure $CsPbBr_3$ and OLA-$CsPbBr_3$ are measured to investigate the interfacial optoelectric properties of the perovskite crystals. As indicated in **Figure 5**a,b, the top of valence band for OLA-$CsPbBr_3$ is shifted to a lower binding energy region by $\Delta E = 1.21 - 1.08 = 0.13$ eV compared with pure $CsPbBr_3$. The optical absorption spectra of pure $CsPbBr_3$ and OLA-$CsPbBr_3$ are shown in Figure 5c. It indicates that their optical absorption band edges are overlapped well and with a value equal to 2.37 eV. Therefore, we can draw the energy level diagram of pure $CsPbBr_3$ and OLA-$CsPbBr_3$ based on the above results, as shown in Figure 5d. It can be seen that the energy level diagram of OLA-$CsPbBr_3$ changes slightly than the pure $CsPbBr_3$ crystal. This evidence further suggests that the OLA molecules can influence the surface of perovskite by modifying the interfacial physical properties.

## 2.4. Luminescence Stability

To further investigate the luminescent stability of perovskite, we also measured the PL performance of pure $CsPbBr_3$ microplate before and after passivation. **Figure 6**a shows the time-dependent PL intensities of a pure $CsPbBr_3$ microplate excited by a 405 nm continuous laser beam with a fluence of $2.442 \times 10^3$ mJ cm$^{-2}$.
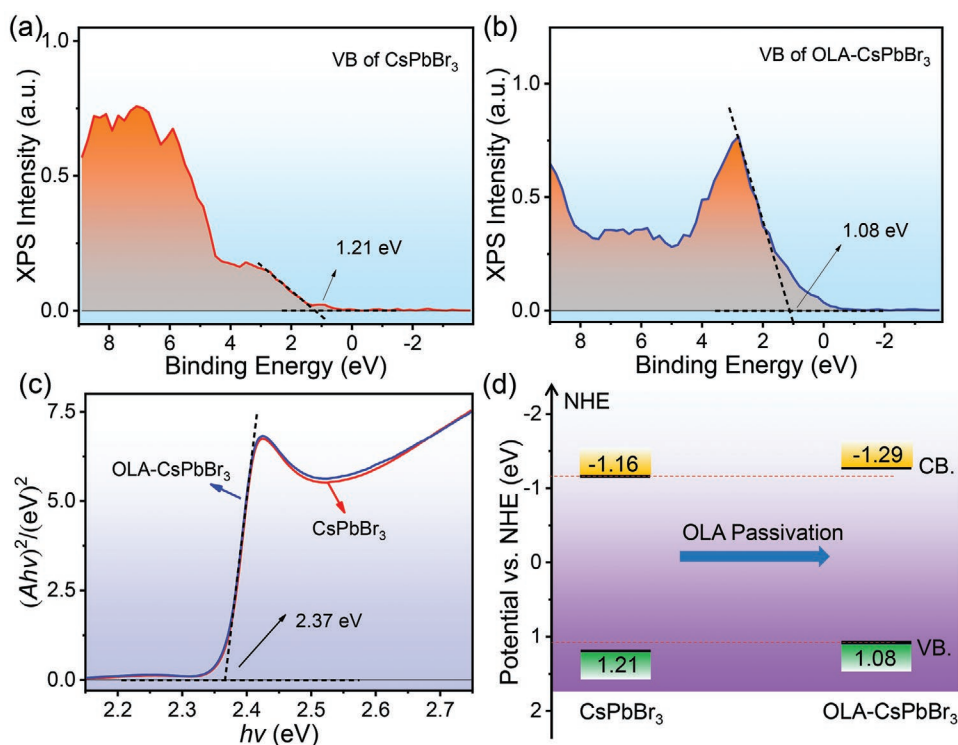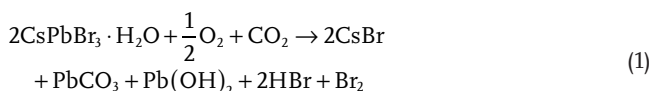
**Figure 5.** XPS valence band spectra of a) pure $CsPbBr_3$ and b) OLA-$CsPbBr_3$. c) Absorptance of pure $CsPbBr_3$ and OLA-$CsPbBr_3$. d) Energy level diagram of pure $CsPbBr_3$ and OLA-$CsPbBr_3$.

As shown in Figure 6a, the pure $CsPbBr_3$ microcrystal exhibits poor luminescent performance and stability. However, with the passivation of undercoordinated Pb atoms at surface of the pure $CsPbBr_3$ microplate by OLA, the performance of luminescent stability for OLA-$CsPbBr_3$ significantly enhanced, as indicated in Figure 6b. It shows that the luminescence stability of perovskite can be significantly improved through the passivation of undercoordinated Pb atoms with OLA molecules. As reported in the literature, the photodegraded reactions of $CsPbBr_3$ crystals under light illumination in an atmospheric environment are expressed as follows:[47,48,61]

$$2CsPbBr_3 \cdot H_2O + \frac{1}{2}O_2 + CO_2 \rightarrow 2CsBr$$
$$+ PbCO_3 + Pb(OH)_2 + 2HBr + Br_2 \tag{1}$$

$$Pb(OH)_2 \rightarrow +PbO + H_2O \tag{2}$$

To begin, an $H_2O$ molecule can be absorbed by an active site (such as surface lattice defect, etc.) to form $CsPbBr_3 \cdot H_2O$.[47,48] Subsequently, photodegraded reactions can be switched on with $CO_2$ and $O_2$ molecules under light illumination. Because the reaction destroys the structure of perovskite crystals, the luminescent performance of $CsPbBr_3$ microcrystal decrease gradually.

Combined with the above results and analysis, we obtained the possible mechanism for the improvement of the luminescence stability of perovskite with OLA molecules, as presented in Figure 6c. It has been reported that,[62] the O atom of $H_2O$ molecule is preferred to bond with a $Pb^{2+}$ undercoordinated

bond at the perovskite surface with a bond length of 2.53 Å and a binding energy of 808 meV. Since large numbers of undercoordinated $Pb^{2+}$ bonds offer adsorption sites for $H_2O$ molecules, structural degradation of perovskite can be accelerated by photodegraded reactions. However, when the crystal was coated with OLA molecules, the undercoordinated $Pb^{2+}$ bonds can be passivated by a lone pair of N atoms in OLA molecules. The binding energy of the Pb atom to OLA is 874 meV,[61] which is much higher than the $H_2O$ molecule (808 meV). We noticed that room-temperature thermal energy is about 26 meV ($k_BT$, $T$ = 300 K). However, the $H_2O$ molecule is still not enough to destroy the binding energy of lead-halogen bond between the N atom and Pb atom when it accepts the thermal energy ($k_BT$) at room temperature. Therefore, OLA molecules can not only passivate abundant undercoordinated $Pb^{2+}$ bonds but also inhibit photodegradation reactions and enhance the luminescence stability of perovskite crystals.

## 3. Conclusion

To conclude, in this work, OLA molecules were employed to passivate the surface defects of pure $CsPbBr_3$ microplate and improved its luminescent performance. With the similar passivation mechanism of Lewis bases, OLA molecules can effectively passivate the uncoordinated $Pb^{2+}$ chemical bonds at the surface of perovskite. Hence, the PL intensity and PL lifetime were enhanced significantly with the decrease of surface trap states. In addition, the luminescence stability of OLA-$CsPbBr_3$ was improved remarkably by inhibiting photodegradation
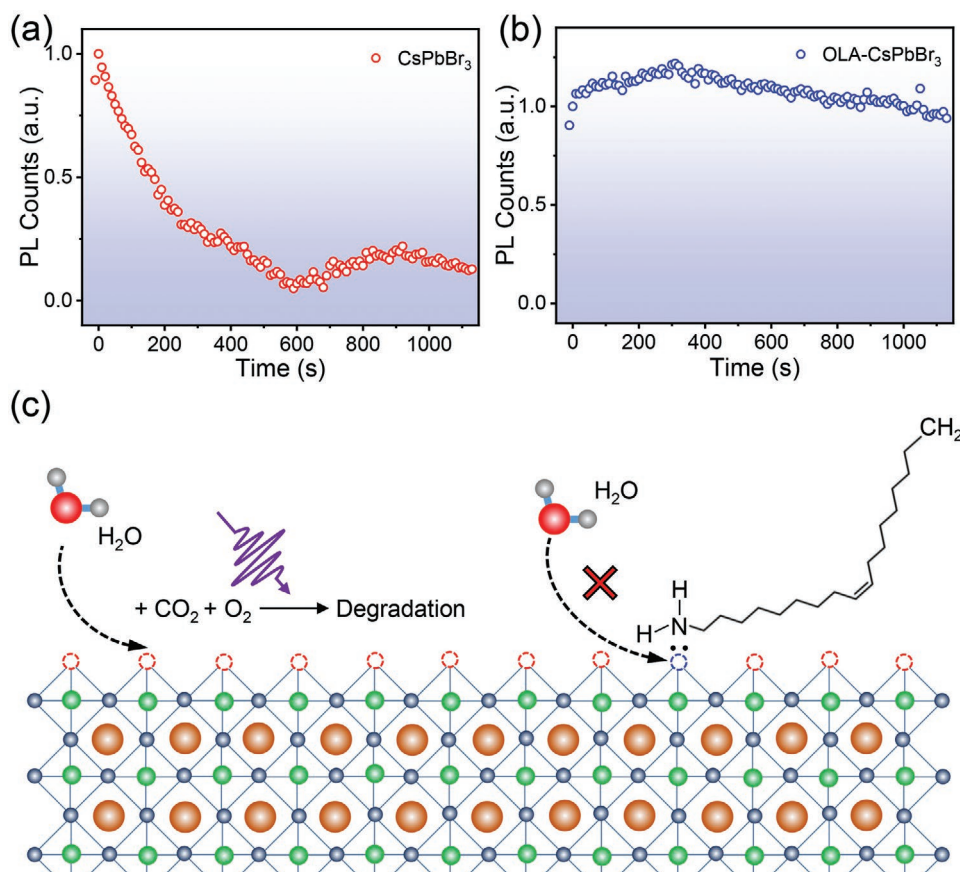
**ADVANCED
SCIENCE NEWS**

www.advancedsciencenews.com

**ADVANCED
OPTICAL
MATERIALS**

www.advopticalmat.de

**Figure 6.** Luminescent stability for a) pure CsPbBr$_3$ and b) OLA-CsPbBr$_3$. The excitation source is a 405 nm continuous laser beam and the fluence is fixed at $2.44 \times 10^3$ mJ cm$^{-2}$. c) The possible photodegradation mechanism for OLA molecules at the surface of pure CsPbBr$_3$ microplate.

reactions with H$_2$O molecules. Our results not only deepen the understanding of the surface passivation mechanism but also can be applied to a wide range of luminescent materials and devices.

## Supporting Information

Supporting Information is available from the Wiley Online Library or from the author.

## Conflict of Interest

The authors declare no conflict of interest.

## Data Availability Statement

The data that support the findings of this study are available from the corresponding author upon reasonable request.

[1] A. Kojima, K. Teshima, Y. Shirai, T. Miyasaka, *J. Am. Chem. Soc.* **2009**, *131*, 6050.

[2] H. Zhou, Q. Chen, G. Li, S. Luo, T.-b. Song, H.-S. Duan, Z. Hong, J. You, Y. Liu, Y. Yang, *Science* **2014**, *345*, 542.

[3] M. Saliba, T. Matsui, K. Domanski, J.-Y. Seo, A. Ummadisingu, S. M. Zakeeruddin, J.-P. Correa-Baena, W. R. Tress, A. Abate, A. Hagfeldt, M. Gratzel, *Science* **2016**, *354*, 206.

[4] J. Y. Kim, J. W. Lee, H. S. Jung, H. Shin, N. G. Park, *Chem. Rev.* **2020**, *120*, 7867.

[5] L. Hu, Q. Zhao, S. Huang, J. Zheng, X. Guan, R. Patterson, J. Kim, L. Shi, C.-H. Lin, Q. Lei, D. Chu, W. Tao, S. Cheong, R. D. Tilley, A. W. Y. Ho-Baillie, J. M. Luther, J. Yuan, T. Wu, *Nat. Commun.* **2021**, *12*, 466.

[6] M. De Bastiani, A. J. Mirabelli, Y. Hou, F. Gota, E. Aydin, T. G. Allen, J. Troughton, A. S. Subbiah, F. H. Isikgor, L. Liu, L. Xu, B. Chen, E. Van Kerschaver, D. Baran, B. Fraboni, M. F. Salvador, U. W. Paetzold, E. H. Sargent, S. De Wolf, *Nat. Energy* **2021**, *6*, 167.

[7] L. Shi, K. Chen, A. Zhai, G. Li, M. Fan, Y. Hao, F. Zhu, H. Zhang, Y. Cui, *Laser Photonics Rev.* **2021**, *15*, 2000401.

[8] W. Tian, H. Zhou, L. Li, *Small* **2017**, *13*, 1702107.

[9] H.-P. Wang, S. Li, X. Liu, Z. Shi, X. Fang, J.-H. He, *Adv. Mater.* **2021**, *33*, 2003309.

[10] D. Liu, B.-B. Yu, M. Liao, Z. Jin, L. Zhou, X. Zhang, F. Wang, H. He, T. Gatti, Z. He, *ACS Appl. Mater. Interfaces* **2020**, *12*, 30530.

[11] Y. Zou, F. Li, C. Zhao, J. Xing, Z. Yu, W. Yu, C. Guo, *Adv. Opt. Mater.* **2019**, *7*, 1900676.

[12] J. W. Ward, H. L. Smith, A. Zeidell, P. J. Diemer, S. R. Baker, H. Lee, M. M. Payne, J. E. Anthony, M. Guthold, O. D. Jurchescu, *ACS Appl. Mater. Interfaces* **2017**, *9*, 18120.

[13] H. Sun, T. Lei, W. Tian, F. Cao, J. Xiong, L. Li, *Small* **2017**, *13*, 1701042.

[14] J. J. Yoo, G. Seo, M. R. Chua, T. G. Park, Y. Lu, F. Rotermund, Y.-K. Kim, C. S. Moon, N. J. Jeon, J.-P. Correa-Baena, V. Bulovic, S. S. Shin, M. G. Bawendi, J. Seo, *Nature* **2021**, *590*, 587.

[15] J. Jeong, M. Kim, J. Seo, H. Lu, P. Ahlawat, A. Mishra, Y. Yang, M. A. Hope, F. T. Eickemeyer, M. Kim, Y. J. Yoon, I. W. Choi, B. P. Darwich, S. J. Choi, Y. Jo, J. H. Lee, B. Walker, S. M. Zakeeruddin, L. Emsley, U. Rothlisberger, A. Hagfeldt, D. S. Kim, M. Graetzel, J. Y. Kim, *Nature* **2021**, *592*, 381.

[16] E. Lamanna, F. Matteocci, E. Calabrò, L. Serenelli, E. Salza, L. Martini, F. Menchini, M. Izzi, A. Agresti, S. Pescetelli, S. Bellani, A. E. Del Río Castillo, F. Bonaccorso, M. Tucci, A. Di Carlo, *Joule* **2020**, *4*, 865.

[17] B. R. Sutherland, E. H. Sargent, *Nat. Photonics* **2016**, *10*, 295.

[18] Y. J. Yoon, Y. S. Shin, H. Jang, J. G. Son, J. W. Kim, C. B. Park, D. Yuk, J. Seo, G. H. Kim, J. Y. Kim, *Nano Lett.* **2021**, *21*, 3473.

[19] S.-J. Woo, J. S. Kim, T.-W. Lee, *Nat. Photonics* **2021**, *15*, 630.

[20] G. Pacchioni, *Nat. Rev. Mater.* **2021**, *6*, 108.

[21] H. Yu, X. Xu, H. Liu, Y. Wan, X. Cheng, J. Chen, Y. Ye, L. Dai, *ACS Nano* **2020**, *14*, 552.

[22] K. Wang, S. Wang, S. Xiao, Q. Song, *Adv. Opt. Mater.* **2018**, *6*, 1800278.

[23] G. Li, T. Che, X. Ji, S. Liu, Y. Hao, Y. Cui, S. Liu, *Adv. Funct. Mater.* **2019**, *29*, 1805553.

[24] S. W. Eaton, M. Lai, N. A. Gibson, A. B. Wong, L. Dou, J. Ma, L. W. Wang, S. R. Leone, P. Yang, *Proc. Natl. Acad. Sci. USA* **2016**, *113*, 1993.

[25] T. C. Sum, N. Mathews, *Energy Environ. Sci.* **2014**, *7*, 2518.

[26] L. Chouhan, S. Ghimire, C. Subrahmanyam, T. Miyasaka, V. Biju, *Chem. Soc. Rev.* **2020**, *49*, 2869.

[27] H. Chen, S. Xiang, W. Li, H. Liu, L. Zhu, S. Yang, *Sol. RRL* **2018**, *2*, 1700188.

[28] Q. Zhang, S. Zuo, P. Chen, C. Pan, *Infomat* **2021**, *3*, 987.

[29] C. Wang, R. Ma, D. Peng, X. Liu, J. Li, B. Jin, A. Shan, Y. Fu, L. Dong, W. Gao, Z. L. Wang, C. Pan, *Infomat* **2021**, *3*, 1272.

[30] J. Li, Z. Yuan, X. Han, C. Wang, Z. Huo, Q. Lu, M. Xiong, X. Ma, W. Gao, C. Pan, *Small Sci.* **2022**, *2*, 2100083.

[31] T. A. S. Doherty, A. J. Winchester, S. Macpherson, D. N. Johnstone, V. Pareek, E. M. Tennyson, S. Kosar, F. U. Kosasih, M. Anaya, M. Abdi-Jalebi, Z. Andaji-Garmaroudi, E. L. Wong, J. Madeo, Y. H. Chiang, J. S. Park, Y. K. Jung, C. E. Petoukhoff, G. Divitini, M. K. L. Man, C. Ducati, A. Walsh, P. A. Midgley, K. M. Dani, S. D. Stranks, *Nature* **2020**, *580*, 360.

[32] Z. Ni, C. Bao, Y. Liu, Q. Jiang, W.-Q. Wu, S. Chen, X. Dai, B. Chen, B. Hartweg, Z. Yu, Z. Holman, J. Huang, *Science* **2020**, *367*, 1352.

[33] X. Han, Z. Xu, W. Wu, X. Liu, P. Yan, C. Pan, *Small Struct.* **2020**, *1*, 2000029.

[34] J. Ren, W. Zhang, Y. Wang, Y. Wang, J. Zhou, L. Dai, M. Xu, *Infomat* **2019**, *1*, 396.

[35] Y. Lu, X. Qu, W. Zhao, Y. Ren, W. Si, W. Wang, Q. Wang, W. Huang, X. Dong, *Research* **2020**, *2020*, 2038560.

[36] G. Ge, W. Yuan, W. Zhao, Y. Lu, Y. Zhang, W. Wang, P. Chen, W. Huang, W. Si, X. Dong, *J. Mater. Chem. A* **2019**, *7*, 5949.

[37] G. Ge, Y. Lu, X. Qu, W. Zhao, Y. Ren, W. Wang, Q. Wang, W. Huang, X. Dong, *ACS Nano* **2020**, *14*, 218.

[38] A. Walsh, D. O. Scanlon, S. Chen, X. G. Gong, S.-H. Wei, *Angew. Chem., Int. Ed.* **2015**, *54*, 1791.

[39] J. Kang, L. W. Wang, *J. Phys. Chem. Lett.* **2017**, *8*, 489.

[40] Q. Jiang, Y. Zhao, X. Zhang, X. Yang, Y. Chen, Z. Chu, Q. Ye, X. Li, Z. Yin, J. You, *Nat. Photonics* **2019**, *13*, 460.

[41] Y. Zhu, Q. Cui, J. Chen, F. Chen, Z. Shi, X. Zhao, C. Xu, *ACS Appl. Mater. Interfaces* **2021**, *13*, 6820.

[42] Y. Zhu, H. Guo, Q. Cui, J. Chen, Z. Li, J. Lu, T. Lu, Z. Peng, C. Xu, C. Pan, *Laser Photonics Rev.* **2023**, *17*, 2200497.

[43] H. Jin, E. Debroye, M. Keshavarz, I. G. Scheblykin, M. B. J. Roeffaers, J. Hofkens, J. A. Steele, *Mater. Horiz.* **2020**, *7*, 397.

[44] M. Zhou, W. Wang, J. Lu, Z. Ni, *Nano Res.* **2020**, *14*, 29.

[45] D. Zhang, Y. Fu, H. Zhan, C. Zhao, X. Gao, C. Qin, L. Wang, *Light Sci Appl* **2022**, *11*, 69.

[46] D. J. Slotcavage, H. I. Karunadasa, M. D. McGehee, *ACS Energy Lett.* **2016**, *1*, 1199.

[47] Y. Ouyang, L. Shi, Q. Li, J. Wang, *Small Methods* **2019**, *3*, 1900154.

[48] Y. Ouyang, Y. Li, P. Zhu, Q. Li, Y. Gao, J. Tong, L. Shi, Q. Zhou, C. Ling, Q. Chen, Z. Deng, H. Tan, W. Deng, J. Wang, *J. Mater. Chem. A* **2019**, *7*, 2275.

[49] G. Xing, N. Mathews, S. S. Lim, N. Yantara, X. Liu, D. Sabba, M. Gratzel, S. Mhaisalkar, T. C. Sum, *Nat. Mater.* **2014**, *13*, 476.

[50] Y. Zhu, J. Chen, Q. Cui, H. Guo, Z. Li, Z. Shi, C. Xu, *Nano Res.* **2021**, *14*, 4288.

[51] D. Meroni, L. Lo Presti, G. Di Liberto, M. Ceotto, R. G. Acres, K. C. Prince, R. Bellani, G. Soliveri, S. Ardizzone, *J. Phys. Chem. C* **2017**, *121*, 430.

[52] A. Zakhtser, A. Naitabdi, R. Benbalagh, F. Rochet, C. Salzemann, C. Petit, S. Giorgio, *ACS Nano* **2021**, *15*, 4018.

[53] J. Yu, M. Guan, F. Li, Z. Zhang, C. Wang, C. Shu, H. Wei, X.-E. Zhang, *Chem. Commun.* **2012**, *48*, 11011.

[54] S. Liu, Z. Duan, C. He, X. Xu, T. Li, Y. Li, X. Li, Y. Wang, L. Xu, *RSC Adv.* **2018**, *8*, 8026.

[55] T. Huang, S. Mao, G. Zhou, Z. Zhang, Z. Wen, X. Huang, S. Ci, J. Chen, *Nanoscale* **2015**, *7*, 1301.

[56] K. Xu, E. T. Vickers, L. Rao, S. A. Lindley, A. L. C. Allen, B. Luo, X. Li, J. Z. Zhang, *Chemistry* **2019**, *25*, 5014.

[57] B. Chen, P. N. Rudd, S. Yang, Y. Yuan, J. Huang, *Chem. Soc. Rev.* **2019**, *48*, 3842.

[58] Y. Li, H. Wu, W. Qi, X. Zhou, J. Li, J. Cheng, Y. Zhao, Y. Li, X. Zhang, *Nano Energy* **2020**, *77*, 105237.

[59] N. K. Noel, A. Abate, S. D. Stranks, E. S. Parrott, V. M. Burlakov, A. Goriely, H. J. Snaith, *ACS Nano* **2014**, *8*, 9815.

[60] G. Wu, R. Liang, M. Ge, G. Sun, Y. Zhang, G. Xing, *Adv. Mater.* **2022**, *34*, 2105635.

[61] J. Li, L. Wang, X. Yuan, B. Bo, H. Li, J. Zhao, X. Gao, *Mater. Res. Bull.* **2018**, *102*, 86.

[62] B. Akbali, G. Topcu, T. Guner, M. Ozcan, M. M. Demir, H. Sahin, *Phys. Rev. Mater.* **2018**, *2*, 034601.